Inorganic Chemistry

pubs.acs.org/IC

Article

meso-Substitution Activates Oxoiron(IV) Porphyrin π-Cation Radical Complex More Than Pyrrole-β-Substitution for Atom Transfer Reaction

Nami Fukui, Kanako Ueno, Masahiko Hada, and Hiroshi Fujii*

Cite This: *Inorg. Chem.* 2021, 60, 3207−3217

Read Online

ACCESS | Metrics & More | Article Recommendations | Supporting Information

ABSTRACT: There have been two known categories of porphyrins: a *meso*-substituted porphyrin like *meso*-tetramesitylporphyrin (TMP) and a pyrrole-β-substituted porphyrin like native porphyrins and 2,7,12,17-tetramethyl-3,8,13,18-tetramesitylporphyrin (TMTMP). To reveal the chemical and biological function of native hemes, we compare the reactivity of the oxoiron(IV) porphyrin π-cation radical complex (Compound I) of TMP (**TMP-I**) with that of TMTMP (**TMTMP-I**) for epoxidation, hydrogen abstraction, hydroxylation, sulfoxidation, and demethylation reactions. Kinetic analysis of these reactions indicated that **TMP-I** is much more reactive than **TMTMP-I** when the substrate is not sterically bulky. However, as the substrate is sterically bulkier, the difference of the reactivity between **TMP-I** and **TMTMP-I** becomes smaller, and the reactivity of **TMP-I** is comparable to that of **TMTMP-I** for a sterically hindered substrate. Since the redox potential of **TMP-I** is almost the same as that of **TMTMP-I**, we conclude that **TMP-I** is intrinsically more reactive than **TMTMP-I** for these atom transfer reactions, but the steric effect of **TMP-I** is stronger than that of **TMTMP-I**. This is contrary to the previous result for the single electron transfer reaction: **TMTMP-I** is faster than **TMP-I**. DFT calculations indicate that the orbital energies of the Fe═O moiety for **TMTMP-I** are higher than those for **TMP-I**. The difference in steric effect between **TMP-I** and **TMTMP-I** is explained by the distance from the mesityl group to the oxo ligand of Compound I. Significance of the pyrrole-β-substituted structure of the hemes in native enzymes is also discussed on the basis of this study.

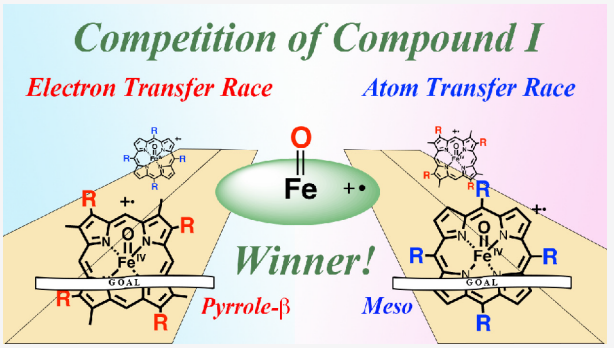

INTRODUCTION

High-valent iron oxo species have been identified as the key intermediates in the reactions of iron-containing catalysts, as well as metalloenzymes.[1−6] The oxoiron(IV) porphyrin π-cation radical species called Compound I and oxoiron(IV) porphyrin species called Compound II have been identified in the catalytic cycles of peroxidases, catalases, and cytochrome P450s.[1−6] Synthetic model complexes of Compound I and Compound II have also been prepared to study the electronic states and reactivity of these complexes.[5,6] Nonheme oxoiron(V) and oxoiron(IV) complexes have also been synthesized by using various synthetic ligand systems.[3] All of these synthetic and enzymatic studies revealed that the reactivity of the high-valent oxoiron species is changed by the structural and electronic effects of the ligands. For example, oxoiron(IV) complexes of 1,4,8,11-tetramethyl-1,4,8,11-tetraazacyclotetradecane have been reported to be stable even at room temperature,[7] but those of tris((*N*-methylbenzimidazol-2-yl)methyl)amine react with cyclohexane even at −40 °C (structures of ligands: see the Appendix in the Supporting Information).[8] Recently, much attention has been directed to reveal how the ligand controls the reactivity of the high-valent iron oxo species and to develop a ligand system that can make the iron oxo species much more reactive.[2,3]

The ligand effect on the reactivity can be seen in heme enzymes. Many heme enzymes have the same heme (iron protoporphyrin IX) but various heme proximal (axial) ligands (e.g., histidine in peroxidases, tyrosine in catalases, and cysteine in cytochrome P450s).[9] The axial ligand is highly conserved in each family having the same biological function.[9] It has been believed that the axial ligand tunes the reactivity of Compound I. Green et al. reported a high pK_a value of the oxo ligand in Compound II of cytochrome P450, and they proposed that it is due to the strong donor effect from the thiolate axial ligand and the origin of the strong oxidizing power of Compound I for hydroxylation of unactivated C−H bonds.[10] We reported a pronounced axial ligand effect of

Received: December 4, 2020
Published: February 15, 2021

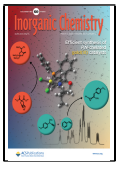

https://dx.doi.org/10.1021/acs.inorgchem.0c03548
Inorg. Chem. 2021, 60, 3207−3217

imidazole and phenolate ligands on the reactivity of synthetic Compound I model complexes; the reactivity increased about 400-fold with the coordination of imidazoles and phenols.[11] The axial ligand effect on Compound I could be explained by the stability of the ground spin state of the product state.[12] A similar axial ligand effect has also been observed for the corrolazine (5,10,15-triazacorrole) ligand system.[13]

A significant ligand effect has been reported not only for the axial ligand but also for the equatorial ligand.[2,3,14−32] The effect of the equatorial ligand has been comprehensively studied by using synthetic porphyrin ligands.[2,3,14−32] These studies revealed that introduction of electron-withdrawing substituents into porphyrin ligands increases reactivity of high-valent oxo species.[14−17,19,21−28] For example, reactivity of Compound I becomes higher as the number of halogen atoms in the *meso*-phenyl group is larger.[14−16,19,22,23] The introduction of the electron-withdrawing substituents increased the redox potentials of Compound I.[22,25−29] Linear correlations could be found between the activation energy and the redox potential of Compound I.[27,28,32] The steric and electronic effect of the substituent changed the selectivity of the oxygen transfer reactions.[24,30,31] These porphyrin ligand effects have been studied by using *meso*-tetraarylporphyrins, in which the sterically hindered aryl groups bind at the *meso*-position of a porphyrin. Groves et al. reported the first example of the synthetic Compound I model complex (**TMP-I**) from *meso*-tetramesitylporphyrin (TMP) shown in Figure 1.[33] However,

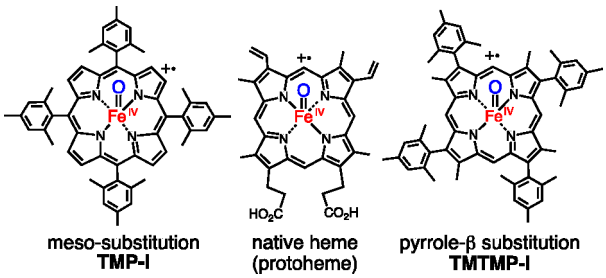

Figure 1. Structures of Compound I of TMP (**TMP-I**), native heme (protoheme), and TMTMP (**TMTMP-I**).

this substitution pattern is different from those of iron porphyrins in native enzymes, in which the substituents bind at the pyrrole-β position of a porphyrin (Figure 1). The synthetic Compound I model complex from a nativelike porphyrin was first synthesized by using 2,7,12,17-tetramethyl-3,8,13,18-tetramesitylporphyrin (TMTMP) shown in Figure 1.[34] The spectroscopic property of Compound I of TMTMP (**TMTMP-I**) was similar to those of Compound I in native enzymes. The redox potential of **TMTMP-I** is very close to that of **TMP-I**; thus, reactivity of **TMTMP-I** was expected to be close to that of **TMP-I**. A previous result of the competitive epoxidation reaction of **TMP-I** and **TMTMP-I** with cyclohexene suggested that reactivity of **TMP-I** is close to that of **TMTMP-I**. However, a recent study on the rate of single electron transfer (ET) reactions showed a significant difference between **TMP-I** and **TMTMP-I**.[35] The ET rates of **TMTMP-I** are 1 to 2 orders magnitude faster than those of **TMP-I**, and the estimated reorganization energy (λ) for **TMP-I** is about 0.2 eV larger than that of **TMTMP-I**. These results suggest that a further study is needed to reveal biological significance of the pyrrole-β-substituted structure of the native hemes in many enzymes.

To clarify whether the reactivity of Compound I is altered by the position of the substituent, the *meso*-position and the pyrrole-β-position, we study here the reactivity of **TMP-I** and **TMTMP-I** toward epoxidation, hydrogen abstraction, hydroxylation, sulfoxidation, and demethylation reactions. The present kinetic study clearly shows that the intrinsic reactivity of **TMP-I** is much higher than that of **TMTMP-I**, but the steric effect of **TMP-I** for these reactions is greater than that of **TMTMP-I**. We conclude that the **TMP-I** is more reactive than **TMTMP-I** for the oxygen- or hydrogen-atom transfer reaction, but **TMTMP-I** is more reactive than **TMP-I** for the single electron transfer reaction. The factors controlling the reactivity and the steric effect for **TMP-I** and **TMTMP-I** are studied from the activation parameters and the DFT calculations.

RESULTS

Epoxidation Reactions. **TMP-I** and **TMTMP-I** were prepared by the oxidation of iron(III) nitrate complexes of TMP and TMTMP with ozone gas at low temperature, respectively.[11,12] The spectroscopic characterizations of **TMP-I** and **TMTMP-I** have been reported previously.[11,16] Figure 2

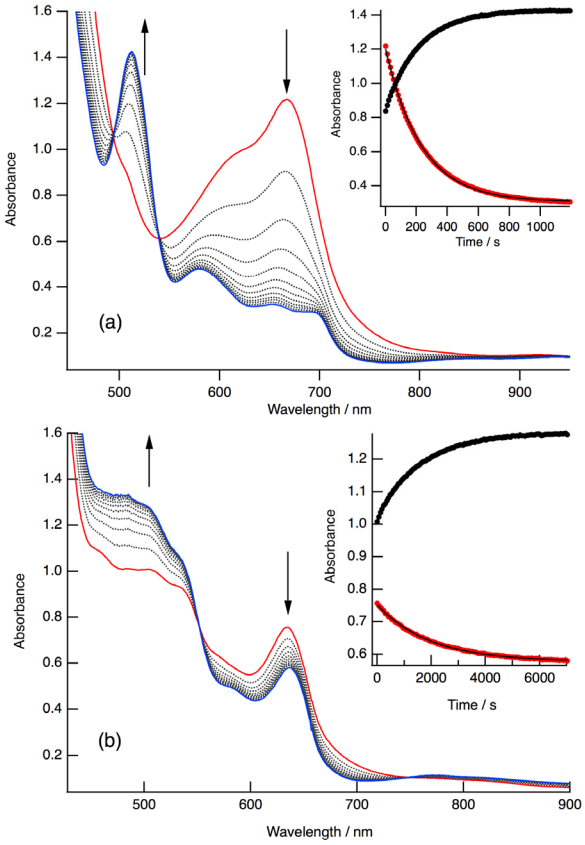

Figure 2. Absorption spectral change for the reactions of (a) TMP-I and (b) TMTMP-I with norbornene in dichloromethane at −50 °C. Red line, immediately after the addition of norbornene; and blue line, after the reaction. Gray broken line, after the addition of norbornene at constant time interval. (a) TMP-I (0.1 mM), norbornene (19.6 mM), and time intervals of 100 s. (b) TMTMP-I (0.1 mM), norbornene (19.9 mM), and time intervals of 585 s. Inset: time course of the absorbance in the reactions. (a) Black circle, at 507 nm; red circle, at 667 nm. (b) Black circle, at 502 nm; red circle, at 632 nm. Solid line: simulation line obtained from a least-squares curve fit with a single exponential function.

https://dx.doi.org/10.1021/acs.inorgchem.0c03548
Inorg. Chem. 2021, 60, 3207−3217

Table 1. Second-Order Rate Constants for the Reactions of TMP-I and TMTMP-I with Olefins in Dichloromethane at −50 °C

substrate	TMP-I $k_2 \times 10^2/M^{-1}\ s^{-1}$ (yield/%)	TMTMP-I $k_2 \times 10^2/M^{-1}\ s^{-1}$ (yield/%)
norbornene	22.0 (86)	1.97 (28)
styrene	2.23	0.538
p-methoxystyrene	86.2 (52)	19.6 (7)
cyclopentene	13.5 (32)	4.59 (18)
cyclohexene	3.89 (68)	1.85 (54)
cyclooctene	2.98 (64)	3.00 (48)

shows the absorption spectral change for the reactions of **TMP-I** and **TMTMP-I** with 200 equiv of norbornene in dichloromethane at −50 °C. With the addition of norbornene, the absorption spectra of **TMP-I** and **TMTMP-I** change to those of their respective initial iron(III) porphyrin complexes. The time courses of the absorbance for the reactions are simulated well with a single-exponential function, providing apparent rate constants. The second-order rate constants were estimated to be $2.20 \times 10^{-1}\ M^{-1}\ s^{-1}$ for **TMP-I** and $1.97 \times 10^{-2}\ M^{-1}\ s^{-1}$ for **TMTMP-I** from the dependence of the rate constants on the concentration of norbornene (Table 1 and Figures S1 and S2). Product analyses of the reaction for **TMP-I** and **TMTMP-I** showed the formation of norbornene oxide in 86% and 28% yields, respectively. The rate constant for **TMP-I** is 1 order magnitude greater than that for **TMTMP-I**. To investigate whether **TMP-I** is more reactive than **TMTMP-I** for other olefins, we examined the epoxidation reactions of styrene, 4-methoxystyrene, cyclopentene, cyclohexene, and cyclooctene (Figures S3 and S4). The second-order rate constants were estimated from the dependence of the apparent rate constants on the concentration of olefins (Figures S5−S14) and are summarized in Table 1. As observed for norbornene, the second-order rate constants of styrene, 4-methoxystyrene, cyclopentene, and cyclohexene for **TMP-I** are larger than those for **TMTMP-I**, but that of cyclooctene for **TMP-I** is almost identical to that for **TMTMP-I**. For cyclic olefins, the reaction rate constant of **TMP-I** is decreased with an increase in the ring size, but that of **TMTMP-I** is unchanged. These results can be explained by the difference of the steric effect between **TMP-I** and **TMTMP-I**. Since the *meso*-position is nearer to the Fe═O moiety than the pyrrole-β position, the reaction space around the oxo ligand of **TMP-I** is smaller than that of **TMTMP-I** (see the Discussion section). The product analyses of these reactions also afforded the corresponding epoxides in moderate yields (Table 1). The yields of the epoxides for **TMP-I** are higher than those for **TMTMP-I**. In addition, **TMP-I** afforded cyclohexene oxide, 2-cyclohexen-1-ol, and 2-cyclohexen-1-one from cyclohexene, but **TMTMP-I** formed only cyclohexene oxide.

Hydrogen Abstraction Reactions. We further compared the reactivity of **TMP-I** with **TMTMP-I** for hydrogen abstraction reactions by using 1,4-cyclohexadiene, 1-methyl-1,4-cyclohexadiene, 1,4-dihydronaphthalene, and 9,10-dihydroanthracene at −50 °C. The absorption spectral changes for the reactions of **TMP-I** with these substrates are shown in Figure S15. As observed for the epoxidation reactions, the absorption spectra of **TMP-I** change to those of the initial iron(III) nitrate complex of TMP with clear isosbestic points upon the addition of these substrates. Product analyses of these reactions showed the formation of the corresponding aromatic compounds in moderate yields (Table 2). The reaction rate constants for the hydrogen abstraction reactions were also estimated from time course of the absorbance, and the second-order rate constants are estimated from the dependence of the rate constant on the concentration of these substrates (Figures S16−S19). The second-order rate constants are summarized in Table 2. The reaction rate constant decreases with an increase in the molecular size of the substrate: 1,4-cyclohexadiene < 1,4-dihydronapthalene < 9,10-dihydroanthracene.

Table 2. Second-Order Rate Constants for the Hydrogen Abstraction and Hydroxylation Reactions of TMP-I and TMTMP-I in Dichloromethane at −50 °C

substrate	TMP-I $k_2/M^{-1}\ s^{-1}$ (yield/%)	TMTMP-I $k_2/M^{-1}\ s^{-1}$ (yield/%)
1,4-cyclohexadiene	5.60 (49)	0.489 (18)
1-methyl-1,4-cyclohexadiene	7.54 (64)	1.45 (22)
1,4-dihydronaphthalene	3.42	4.64
9,10-dihydroanthracene	0.522 (28)	0.461 (<1)
xanthene	1.04 (75)[b]	1.35
tetraline[a]	2.16×10^{-2} (16)	2.77×10^{-2} (1)

[a]At −30 °C. [b]Ref 36.

The absorption spectrum of **TMTMP-I** also changes with clear isosbestic points upon the addition of these substrates, but the absorption spectra of the final reaction products are not identical with that of the initial iron(III) porphyrin complex of TMTMP (Figure S20). The absorption spectra of the final reaction solutions show a new peak around 780 nm, and the new peak becomes significant for 1,4-dihydronaphthalene and 9,10-dihydroanthracene. This peak was not unchanged when tetra-*n*-butylammonium iodide is added to the final reaction solution at −50 °C but changed to the spectrum of an iron(III) porphyrin complex when the final solution was allowed to warm to room temperature. Product analyses indicate that the yields of the corresponding aromatic compounds from the reactions of **TMTMP-I** with 1,4-cyclohexadiene and 1-methyl-1,4-cyclohexadiene are lower than those of **TMP-I**, and no product is obtained from the reaction with 9,10-dihydroanthracene (Table 2). The reaction rate constants for the reactions of **TMTMP-I** with these substrates were also estimated using absorption spectroscopy (Figures S21−S24 and Table 2). The rate constants for **TMTMP-I** with 1,4-cyclohexadiene and 1-methyl-1,4-cyclohexadiene are much smaller than those for **TMP-I**, but the reaction rates of **TMTMP-I** are close to those of **TMP-I** for more sterically hindered substrates such as 1,4-dihydronaphthalene and 9,10-dihydroanthracene.

Hydroxylation Reactions. Previously, we showed that **TMP-I** reacts with xanthene and tetraline to afford xanthydrol and 1,2,3,4-tetrahydro-1-naphthol, respectively.[36] To compare the reactivity of **TMP-I** and **TMTMP-I** for the hydroxylation reaction, we examined the reactions with xanthene and tetraline. With the addition of xanthene, the absorption

https://dx.doi.org/10.1021/acs.inorgchem.0c03548
Inorg. Chem. 2021, 60, 3207−3217

spectrum of **TMP-I** changes to that of the initial iron(III) porphyrin complex with clear isosbestic points, but the absorption spectrum of **TMTMP-I** changes to that of the iron(III) porphyrin complex, concomitant with the formation of the new peak at around 780 nm at −30 °C (Figure S25). These spectral changes were close to those observed for the hydrogen abstraction reactions of 1,4-dihyrdonaphthalene and 9,10-dihyrdoanthracene (Figure S20). The second-order rate constants, estimated from the absorption spectroscopy (Figures S26−S29), are summarized in Table 2. The reaction rates of **TMTMP-I** for xanthene and tetraline are close to those of **TMP-I**. Product analysis showed that the hydroxylation products were produced from the reactions of **TMP-I**, xanthydrol (75%) from xanthene and 1,2,3,4-tetrahydro-1-naphthol (16%) from tetraline, but the hydroxylation products hardly formed from the reactions of **TMTMP-I**. These results are the same as the hydrogen abstraction reactions.

Previously, we reported a significant deuterium kinetic isotope effect (KIE) for the reaction of **TMP-I** with xanthene.[36] The KIE value for xanthene was reported to be 34. To compare the proton transfer process, we further determined the KIE value for **TMTMP-I**. The KIE value for xanthene-d_2 was estimated to be 9.9 (Figure S27), smaller than that of **TMP-I**. These KIE values suggest the participation of H-transfer processes in the rate-limiting steps. The smaller KIE value for **TMTMP-I** would be related to the formation of the complex having a peak at around 780 nm.

Sulfoxidation Reactions. We compared the reactivity of **TMP-I** with **TMTMP-I** for the sulfoxidation reactions of thioanisole and *p*-chlorothioanisole at −80 °C. The reactions were too fast to follow with an absorption spectrometer at −50 °C. **TMP-I** and **TMTMP-I** react with these sulfides to produce the corresponding initial iron(III) porphyrin complexes (Figure S30). The reaction rate constants of these sulfoxidation reactions, estimated from the time courses of the absorbance (Figures S31−S36), are summarized in Table 3.

Table 3. Second-Order Rate Constants for the Reactions of TMP-I and TMTMP-I with Sulfides and *N,N*-Dimethylanilines in Dichloromethane

substrate	$E_{1/2}$/V vs SCE	TMP-I k_2/M^{-1} s^{-1} (yield/%)	TMTMP-I k_2/M^{-1} s^{-1} (yield/%)
thioanisole[a]	1.34[d]	90.7	22.3
p-chlorothioanisole[a]	1.37[d]	55.6	12.9
tert-butyl methylsulfide[b]		3.21×10^2	1.75×10^3
N,N-dimethyl-*p*-nitroaniline[c]	0.96[e]	4.14 (66)	0.919 (32)
N,N-dimethyl-*p*-bromoaniline[b]	0.51[e]	7.33×10^4	9.97×10^5
N,N-dimethylaniline[b]	0.57[e]	1.60×10^5 (63)	very fast (45)

[a]At −80 °C. [b]At −20 °C. [c]At −50 °C. [d]Ref 37. [e]Ref 38.

The sulfoxidation reactions of **TMP-I** with thioanisole and *p*-chlorothioanisole are about 4-fold faster than those of **TMTMP-I**. This is consistent with the results of the epoxidation and hydrogen abstraction reactions for sterically less-hindered substrates. Furthermore, we examined the reactions of **TMP-I** and **TMTMP-I** with *tert*-butyl methyl sulfide to investigate the steric effect. As observed for the other reactions, the reaction of **TMTMP-I** is faster than that of **TMP-I** for *tert*-butyl methyl sulfide (Table 3).

Demethylation Reactions of *N,N*-Dimethylanilines. We also examined the reactions of **TMP-I** and **TMTMP-I** with *N,N*-dimethylanilines. The formation of *N*-methylanilines and their yields from the reactions were confirmed by HPLC analysis of the reaction products. The yields of *N*-methyl-*p*-nitroaniline and *N*-methylaniline are shown in Table 3.

For *N,N*-dimethyl-*p*-nitroaniline, whose redox potential is higher than those of **TMP-I** and **TMTMP-I**, the reactions of **TMP-I** and **TMTMP-I** could be followed with an absorption spectrometer at −50 °C. As observed for other substrates, the absorption spectra of **TMP-I** and **TMTMP-I** change to those of the corresponding iron(III) porphyrin complexes with clear isosbestic points (Figure S37). The second-order rate constants, estimated from the absorption spectral change (Figures S38 and S39), are shown in Table 3. The reaction rate of **TMP-I** is larger than that of **TMTMP-I**.

For the reactions with *N,N*-dimethylaniline and *N,N*-dimethyl-*p*-bromoaniline, whose redox potentials are lower than those of **TMP-I** and **TMTMP-I**, we followed the reactions using a rapid-mixing stopped flow system at −20 °C because the reactions were too fast to follow with an ordinary absorption spectrometer. The absorption spectral changes for the reactions of **TMP-I** and **TMTMP-I** with *N,N*-dimethyl-*p*-bromoaniline and *N,N*-dimethylaniline are shown in Figure S37. The absorption spectral changes show the formation of the iron(III) porphyrin complex with clear isosbestic points within 100 ms after mixing of **TMP-I** with *N,N*-dimethyl-*p*-bromoaniline and *N,N*-dimethylaniline, and mixing of **TMTMP-I** with *N,N*-dimethyl-*p*-bromoaniline. No intermediate is detected in the reactions, indicating that the initial step, the step from Compound I to Compound II, is the rate-limiting step for these demethylation reactions. The second-order rate constants estimated from the absorption spectral changes for these reactions (Figures S40−S42) are summarized in Table 3. However, a reliable second-order rate constant cannot be estimated for the reaction of **TMTMP-I** with *N,N*-dimethylaniline. The reaction was too fast to follow even with a stopped flow system, and only the last process of the reaction could be observed (Figure S37). Moreover, the absorption spectral change for the reaction of **TMTMP-I** with *N,N*-dimethylaniline is different from those of other demethylation reactions; the spectral change for **TMTMP-I** results from the reaction from Compound II to iron(III) porphyrin, but those for other reactions result from the reaction from Compound I to iron(III) porphyrin. The rate-limiting step for the reaction of **TMTMP-I** with *N,N*-dimethylaniline changes to the step from Compound II to iron(III) porphyrin. Therefore, the estimated reaction rate for the reaction of **TMTMP-I** with *N,N*-dimethylaniline cannot compare directly with the rates for other reactions. The reaction rate from Compound I to Compound II for the reaction of **TMTMP-I** with *N,N*-dimethylaniline would be much larger than the reaction rate ($\sim 3 \times 10^5$ M^{-1} s^{-1}) estimated from the observed spectral change from Compound II to iron(III) porphyrin.

To study the reaction mechanism, we studied the deuterium KIE for the demethylation reactions. The kinetic data for the reactions of **TMP-I** and **TMTMP-I** with deuterium labeled *N,N*-dimethyl-*p*-nitroaniline are summarized in Figures S43 and S44. The estimated KIE values, k_H/k_D, for the reactions of **TMP-I** and **TMTMP-I** with *N,N*-dimethyl-*p*-nitroaniline were 4.4 and 2.1, respectively. These KIE values suggest the participation of H-transfer processes in the rate-limiting steps.

https://dx.doi.org/10.1021/acs.inorgchem.0c03548
Inorg. Chem. 2021, 60, 3207−3217

As observed for the hydroxylation reaction, the KIE value for **TMTMP-I** was smaller than that for **TMP-I** and can be related to the formation of the complex having the peak at around 780 nm.

Activation Parameters. In order to obtain information on the transition states of the reactions of **TMP-I** and **TMTMP-I**, we estimated the activation parameters for the hydrogen abstraction reaction of 1,4-cyclohexadiene from the reaction rates in the temperature range from −50 to −80 °C. Eyring plots for these reactions are shown in Figure 3, and the

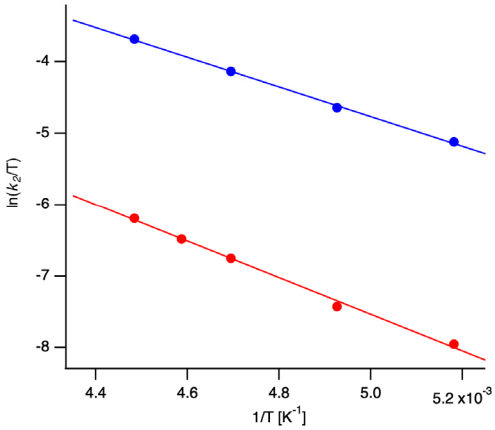

Figure 3. Eyring plots for the reactions of **TMP-I** (blue) and **TMTMP-I** (red) with 1,4-cyclohexadiene in dichloromethane. The solid lines indicate the simulation of the least-squares fits with a linear function.

enthalpy of activation ($\Delta H^{\ddagger}$) and the entropy of activation ($\Delta S^{\ddagger}$) calculated from the Eyring plots are 17.7 kJ mol^{-1} and −148.8 J K^{-1} mol^{-1} for **TMP-I** and 21.2 kJ mol^{-1} and −154.4 J K^{-1} mol^{-1} for **TMTMP-I**, respectively. The $\Delta H^{\ddagger}$ value for **TMP-I** is 3.5 kJ mol^{-1} smaller than that for **TMTMP-I**, and the $|\Delta S^{\ddagger}|$ value for **TMP-I** is 6.0 J K^{-1} mol^{-1} smaller than for **TMTMP-I**. The negative $\Delta S^{\ddagger}$ values indicate the associative rate-limiting step for the hydrogen abstraction reaction; Compound I and the substrate tightly bind in the transition state. The $\Delta S^{\ddagger}$ values for the hydrogen abstraction reactions are larger than those for the epoxidation reactions but close to those of hydroxylation reactions. The $-T\ \Delta S^{\ddagger}$ values at a temperature over 140 K are larger than the $\Delta H^{\ddagger}$ values, indicating the entropy control for the hydrogen abstraction reaction. The free energy of activation ($\Delta G^{\ddagger}$) for **TMP-I** is smaller than that for **TMTMP-I**, indicating that **TMP-I** is more reactive than **TMTMP-I** at any reaction temperature.

DFT Calculations. To explain the difference of the reactivity between **TMP-I** and **TMTMP-I**, we performed density functional theory (DFT) calculations. Details of the DFT calculations are described in the Experimental Section. Optimized structures of the model complexes and their bond lengths and bond angles are shown in Figure S45 and Table S1, respectively. Figure 4 shows energies of molecular orbitals near the HOMO and iron d orbitals. The energies of these orbitals are summarized in Tables S2 and S3. These model complexes have lower symmetry than the D_{4h} because of the substitution of the porphyrin ring and the coordination of the axial ligand, but we here denote the molecular orbitals with symmetry labels of the D_{4h} symmetry. The ground states of the model complexes for **TMP-I** and **TMTMP-I** are calculated to be the quartet (S = 3/2) state having unpaired electrons in d_{xz}, d_{yz},

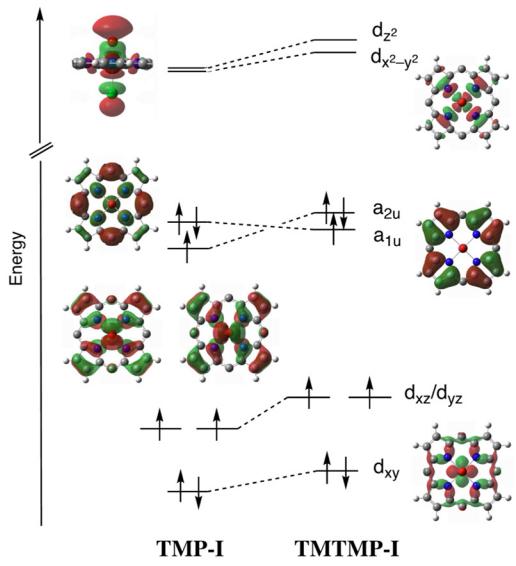

Figure 4. Comparison of orbital energies of **TMP-I** and **TMTMP-I** estimated by the DFT calculation. The average of the orbital energies for the α-spin and β-spin are used for the orbital energies of occupied orbitals.

and porphyrin π orbitals. The unpaired electrons of porphyrin ligands in **TMP-I** and **TMTMP-I** are calculated to occupy the a_{2u} and a_{1u} orbitals, respectively (Figure S46). These results are consistent with the previous spectroscopic studies, indicating the accuracy of the present calculations.[16,39] The energy of the a_{2u} orbital for **TMP-I** is just slightly lower than that of the a_{1u} orbital for **TMTMP-I**. This is consistent with the previous result that the redox potential of **TMP-I** is almost the same as that of **TMTMP-I**. On the other hand, the calculated energies of the iron d orbitals for **TMP-I** are eventually lower than those of **TMTMP-I** (Figure 4 and Table S2). Since the energies of the iron d orbitals are modulated by the energies of the occupied porphyrin orbitals interacting with these iron d orbitals, these results suggest that the energies of the occupied porphyrin orbitals for TMP are lower than those for TMTMP. This is confirmed by the DFT calculations of free bases of TMP and TMTMP (Table S3). The calculated energies of the occupied orbitals, interacting with the iron d orbitals, for the free base of TMTMP are higher than those for TMP. The difference of the energies of these porphyrin orbitals would result from the difference of the electron densities between the *meso*-position and the pyrrole-β-position. When significant electron density is present at the substituted position, the porphyrin orbital is destabilized due to the electronic repulsion between the porphyrin and the substituent. This is confirmed by the electron distribution of these porphyrin orbitals shown in Table S3.

DISCUSSION

Comparison of Reactivity between TMP-I and TMTMP-I. To compare the reactivity between **TMP-I** and **TMTMP-I** for various substrates studied here, we calculated logarithms of the values for the second-order rate constants of **TMP-I** over those of **TMTMP-I**, $\log(k_{\text{TMP-I}}/k_{\text{TMTMP-I}})$. The calculated results are summarized in Figures 5, 7, and 8. The $\log(k_{\text{TMP-I}}/k_{\text{TMTMP-I}})$ value becomes positive when **TMP-I** is more reactive than **TMTMP-I**, but the value becomes negative when **TMTMP-I** is more reactive than **TMP-I**. As shown in

https://dx.doi.org/10.1021/acs.inorgchem.0c03548
Inorg. Chem. 2021, 60, 3207−3217

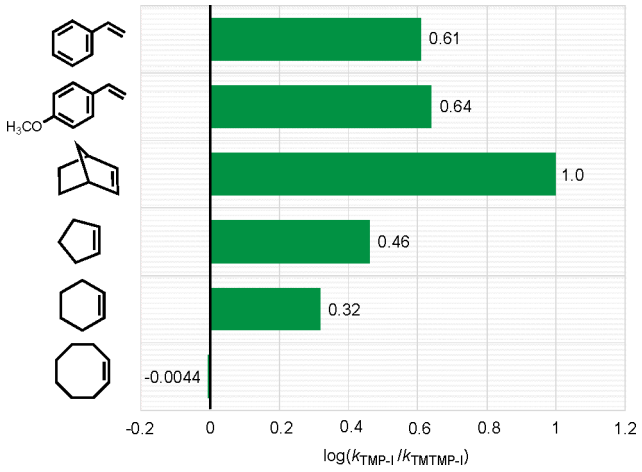

Figure 5. Comparison of the reactivity of **TMP-I** with **TMTMP-I** for the epoxidation reaction. The numbers in the figure are $\log(k_{\text{TMP-I}}/k_{\text{TMTMP-I}})$ values.

Figure 5, the $\log(k_{\text{TMP-I}}/k_{\text{TMTMP-I}})$ values for the epoxidation reactions are positive except for cyclooctene (almost 0). As the size of the cyclic olefin is larger, the $\log(k_{\text{TMP-I}}/k_{\text{TMTMP-I}})$ value for cyclic olefin becomes smaller. These results would be explained by the difference of the steric effect around the oxo ligand between **TMP-I** and **TMTMP-I** (Figure 6). Since the *o*-

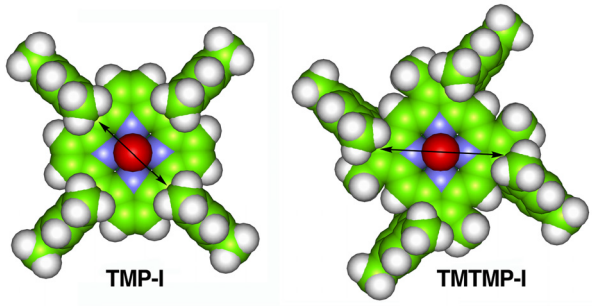

Figure 6. CPK models of the optimized structures of **TMP-I** (left) and **TMTMP-I** (right) by the DFT calculations. The distances between the *o*-methyl carbon atoms facing each other in **TMP-I** and **TMTMP-I** are 9.75 and 11.53 Å, respectively.

methyl group of the mesityl group at the *meso*-position in **TMP-I** is closer to the oxo ligand than that at the pyrrole *β*-position in **TMTMP-I**, the reaction space around the oxo ligand of **TMP-I** is smaller than that of **TMTMP-I**. When the alkene moiety of the substrate is not sterically bulky, the difference of the steric effect hardly affects the reaction rate. Therefore, for such a substrate, the $\log(k_{\text{TMP-I}}/k_{\text{TMTMP-I}})$ value reflects the difference of the intrinsic reactivity between **TMP-I** and **TMTMP-I**; **TMP-I** is more reactive than **TMTMP-I** for the epoxidation reaction. As the substrate is bulkier, the steric effect resulting from the *o*-methyl group of **TMP-I** becomes more significant than that of **TMTMP-I**. This is confirmed by the reaction rates in Table 1. The reaction rate of **TMP-I** for cyclic olefins drastically decreases with an increase in the ring size, while those of **TMTMP-I** do not. All of these results indicate that **TMP-I** is intrinsically more reactive than **TMTMP-I** for the epoxidation reaction although the steric effect of **TMP-I** is stronger than that of **TMTMP-I**.

The above discussion can also be applicable to the hydrogen abstraction and sulfoxidation reactions. As shown in Figures 7

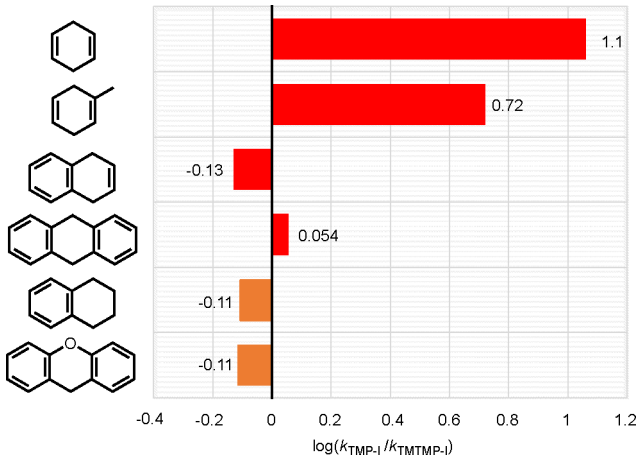

Figure 7. Comparison of the reactivity of **TMP-I** with **TMTMP-I** for the hydrogen abstraction reaction and hydroxylation reaction. The numbers in the figure are $\log(k_{\text{TMP-I}}/k_{\text{TMTMP-I}})$ values.

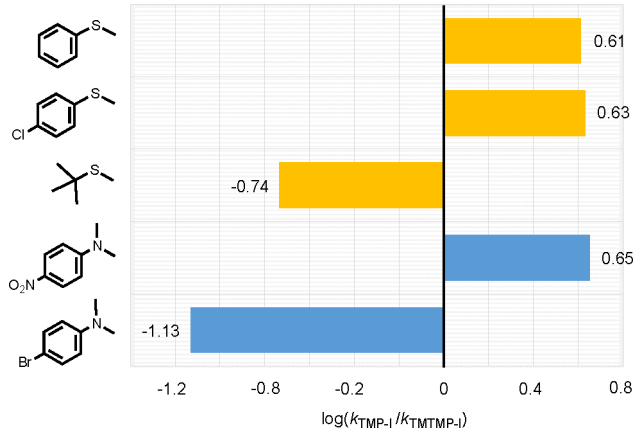

Figure 8. Comparison of the reactivity of **TMP-I** with **TMTMP-I** for the sulfoxidation reaction (yellow bars) and the demethylation reaction (blue bars). The numbers in the figure are $\log(k_{\text{TMP-I}}/k_{\text{TMTMP-I}})$ values.

and 8, the $\log(k_{\text{TMP-I}}/k_{\text{TMTMP-I}})$ values for the hydrogen abstraction and sulfoxidation reactions indicate positive values when the substrates are less hindered. However, the $\log(k_{\text{TMP-I}}/k_{\text{TMTMP-I}})$ values for the sterically hindered substrates such as 1,4-hydronapthalene and 9,10-dihydroanthracene indicate values close to 0, and the large negative value is obtained for *tert*-butyl methyl sulfide. These results clearly indicate that **TMP-I** is intrinsically more reactive than **TMTMP-I** even for the hydrogen abstraction and sulfoxidation reactions although the steric effect of **TMP-I** is stronger than that of **TMTMP-I**. This is also true for the hydroxylation reactions. The $\log(k_{\text{TMP-I}}/k_{\text{TMTMP-I}})$ values are close to 0 for these substrates. Since the structures of tetraline and xanthene are close to those of 1,4-hydronapthalene and 9,10-dihydroanthracene, respectively, these values mainly reflect the difference of the steric effect, rather than the intrinsic reactivity, between **TMP-I** and **TMTMP-I**.

https://dx.doi.org/10.1021/acs.inorgchem.0c03548
Inorg. Chem. 2021, 60, 3207−3217

For the demethylation reactions of *N*,*N*-dimethylanilines, a positive $\log(k_{\text{TMP-I}}/k_{\text{TMTMP-I}})$ value is observed for *N*,*N*-dimethyl-*p*-nitroaniline, while a negative $\log(k_{\text{TMP-I}}/k_{\text{TMTMP-I}})$ value is observed for *N*,*N*-dimethyl-*p*-bromoaniline (Figure 8). The value for *N*,*N*-dimethylaniline would also be negative because the reaction of **TMTMP-I** is faster than that of **TMP-I**. Since these substrates are not sterically bulky, these results cannot be explained by the steric effect as discussed above. These values can be rationalized with the reaction mechanism of the demethylation reactions of these *N*,*N*-dimethylanilines. Previous studies of the demethylation reactions of *N*,*N*-dimethylanilines proposed that the reaction proceeds via the single electron transfer process followed by the H-atom (hydrogen or proton) transfer process.[29,38] When the redox potential of a *N*,*N*-dimethylaniline is lower than that of Compound I (**TMP-I**, 0.88 V; **TMTMP-I**, 0.88 V), the rate-limiting step of the reaction is the electron transfer process from a *N*,*N*-dimethylaniline to Compound I. However, when the redox potential of a *N*,*N*-dimethylaniline is higher than that of Compound I, the rate-limiting step involves the H-atom transfer process. Therefore, the rate-limiting step would be a single electron transfer reaction for *N*,*N*-dimethylaniline and *N*,*N*-dimethyl-*p*-bromoaniline, but it would be the H-atom transfer reaction for *N*,*N*-dimethyl-*p*-nitroaniline. The present KIE values for *N*,*N*-dimethyl-*p*-nitroaniline support this reaction mechanism. The negative $\log(k_{\text{TMP-I}}/k_{\text{TMTMP-I}})$ values for *N*,*N*-dimethyl-*p*-bromoaniline and *N*,*N*-dimethylaniline are consistent with our recent result that **TMTMP-I** is superior to **TMP-I** for the single electron transfer reaction.[35] The positive value for *N*,*N*-dimethyl-*p*-nitroaniline is also reasonable with the present result that **TMP-I** is superior to **TMTMP-I** for the hydrogen abstraction reaction.

The absorption spectral change for the reaction of **TMTMP-I** with *N*,*N*-dimethylaniline suggests the change of the rate-limiting step of the reaction from the electron transfer process to the H-atom transfer process because the redox potential of *N*,*N*-dimethylaniline is lower than that of **TMTMP-I**. The rate constant for the electron transfer reaction of **TMTMP-I** with *N*,*N*-dimethylaniline can be estimated to be 1×10^8 M^{-1} s^{-1} from the redox potential of *N*,*N*-dimethylaniline and a Marcus plot for **TMTMP-I**.[35] The estimated rate supports the change of the rate-limiting step because this rate is much larger than the rate of the demethylation reaction.

All of the present results indicate that **TMP-I** is intrinsically much more reactive than **TMTMP-I** for the epoxidation, hydrogen abstraction, hydroxylation, sulfoxidation, and demethylation reactions while the steric effect of the mesityl group in **TMP-I** is intrinsically more significant than that in **TMTMP-I**. This conclusion seems to conflict with our previous proposal that the reactivity of **TMP-I** is comparative to that of **TMTMP-I**.[16] We deduced this proposal from the absorption spectral change, which showed that both **TMP-I** and **TMTMP-I** react with cyclohexene under the competitive reaction in the **TMP-I** and **TMTMP-I** mixture. This result is also supported by the present individual kinetic analysis (Table 1), where the reaction rate constant of **TMP-I** is close to that of **TMTMP-I** for sterically hindered substrates such as cyclohexene and cyclooctene. As discussed in the above paragraphs, the apparent reactivity of **TMP-I** for cyclohexene accidentally coincides with that of **TMTMP-I** due to a decrease in the reactivity of **TMP-I** by the steric effect.

The reaction mechanisms of Compound I with various substrates have been studied to understand the reactivity of Compound I in many groups. For example, Groves et al. proposed the rebound mechanism for the hydroxylation reaction, in which the hydrogen atom is abstracted from a substrate by the oxo ligand of Compound I, followed by the rebound between the formed iron-bound OH group and the substrate radical.[40,41] The large hydrogen/deuterium kinetic isotope effects for the hydroxylation reactions indicate the participation of the hydrogen abstraction process in the rate-limiting step; the hydrogen atom (one electron−one proton) transfer process is involved in the rate-limiting step of the hydroxylation reaction.[36,42−49] This rate-limiting step can be applicable to the hydrogen abstraction reaction. For the epoxidation reaction, the rate-limiting steps of these mechanisms also involve the electron transfer process and the O−C bond formation process in some manner although many reaction mechanisms have been proposed.[27,32,45,50−52] A previous study for the sulfoxidation reaction with **TMP-I** proposed the direct oxygen atom transfer mechanism.[37] Therefore, the O−S bond formation process and the electron transfer process must be involved in the rate-limiting step. As mentioned in a previous paragraph, the demethylation reaction of *N*,*N*-dimethylaniline proceeds via the single electron transfer process followed by the H-atom (hydrogen or proton) transfer process, and the nature of the rate-limiting step is changed by the redox potential of the aniline.[29,38] Considering a recent study on the single electron transfer reaction and the reaction mechanisms discussed above, we conclude that **TMP-I** is intrinsically much more reactive than **TMTMP-I** when the bond formation process with the oxo ligand is involved in the rate-limiting step while **TMTMP-I** is intrinsically more reactive than **TMP-I** when only the single electron transfer process is involved in the rate-limiting step (Scheme 1).

Scheme 1. Reaction Mechanisms Proposed for the Single Electron Transfer Reaction and the Atom Transfer Reactions

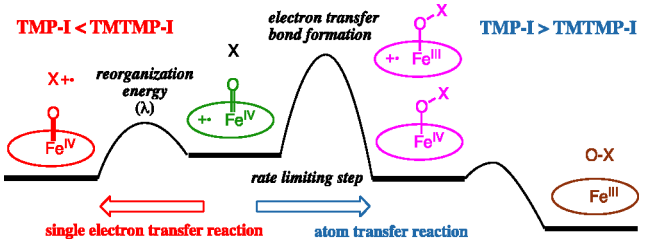

The hydrogen abstraction reaction and hydroxylation reactions of **TMTMP-I** produced a new compound having a peak at around 780 nm. This can be seen in Figures S4, S20, and S25. This compound would be an intermediate that kills or inhibits the hydrogen atom transfer and hydroxylation reactions because the product yields from the reactions are always low when it is observed. The identity of this compound is not clear at present, and further spectroscopic study is required to clarify.

Factors Controlling the Reactivity of Compound I. Numerous previous studies revealed that the redox potential of Compound I is an essential factor for determining the reactivity.[2,3,27,28,32] This is quite reasonable because the electron transfer process is involved in the rate-limiting step of most reactions of Compound I. Linear relationships between the activation energy and the redox potential of high-valent oxo porphyrin species have been reported.[27,28,32]

https://dx.doi.org/10.1021/acs.inorgchem.0c03548
Inorg. Chem. 2021, 60, 3207−3217

However, the redox potential is not the factor for discriminating the intrinsic reactivity of **TMP-I** and **TMTMP-I** because the redox potentials of these complexes are approximately the same.[29]

One of the significant differences between **TMP-I** and **TMTMP-I** is the position of the substituent: the *meso*-substituted porphyrin or the pyrrole β-substituted porphyrin. This structural difference changes the steric effect around the oxo ligand, as discussed in the previous paragraph. However, the steric effect is not the factor for determining the intrinsic reactivity because of the opposite trend to the reactivity. This structural difference also changes the flexibility of the porphyrin ligand. TMTMP is more flexible than TMP because of the absence of the substituent at the *meso*-position. Since the *meso*-position is nearer to the iron center of heme than the pyrrole-β position, the *o*-methyl group of the *meso*-phenyl group at the *meso*-position in TMP induces steric repulsion with the porphyrin plane when the porphyrin plane is deformed, but that of the pyrrole-β position does not. We previously proposed that the flexibility of the porphyrin ring of TMTMP makes the structural change in the single electron transfer reaction easy, decreasing the reorganization energy (λ) and increasing the electron transfer rate.[35] The difference of the reorganization energy between **TMP-I** and **TMTMP-I** is also confirmed by the DFT calculations. The flexibility of the porphyrin ligand would affect the reactivity of Compound I for the O-atom and H-atom transfer reactions. As expected from the large negative value of $\Delta S^{\ddagger}$ for the reaction of Compound I, **TMP-I** and **TMTMP-I** tightly interact with a substrate in the transition state. The flexible porphyrin ring of TMTMP would be unfavorable to have the tight transition state, and the substrate should come closer to the oxo ligand of **TMTMP-I** than **TMP-I** in the transition state. This is also supported by the larger $\Delta H^{\ddagger}$ value for **TMTMP-I**. We propose that the difference of the flexibility of the porphyrin plane makes **TMP-I** more reactive for the atom transfer reaction and **TMTMP-I** more reactive for the single electron transfer reaction.

The difference of the energies of the porphyrin σ and π orbitals would also be another possible factor for changing the reactivity. The present DFT calculations show a significant difference in the energies of the molecular orbitals around the iron-oxo moiety between **TMP-I** and **TMTMP-I** (see Figure 4). The energies of the iron d orbitals for **TMP-I** are lower than those for **TMTMP-I**. As discussed in a previous paragraph, the atom transfer reaction involves the electron transfer process and the bond formation process in the rate-limiting step. Since **TMTMP-I** is faster than **TMP-I** for the single electron transfer process, the reactivity for the atom transfer reaction should be controlled by the bond formation process. The bond formation occurs at the oxo ligand of Compound I, whose orbital is linked to the iron d orbital. Therefore, the stabilization of the iron d orbital would facilitate the bond formation process in the reaction of **TMP-I**, decreasing the activation energy. Since the energies of the iron d orbitals are determined by the orbital energies of the ligands coordinating to the iron, the porphyrin σ and π orbitals interacting with the iron d orbitals should be related to the difference of the reactivity between **TMP-I** and **TMTMP-I**. This is confirmed by the DFT calculations (Table S3). The energies of the porphyrin σ and π orbitals, interacting with the iron d orbitals, for TMP are more stable than those for TMTMP. After all, the difference in the substituted position of the porphyrin ring changes the energies of the porphyrin σ and π orbitals, which further changes the energies of the iron d orbitals, and finally the reactivity of Compound I.

Chemical and Biological Relevance. This study clearly shows that the *meso*-substituted Compound I is more reactive than the pyrrole-β-substituted Compound I for the O-atom and H-atom transfer reactions, but this reactivity is reversed for the single electron transfer reaction. Although further study is needed to support the present results, this study suggests that the *meso*-substituted heme is more suitable than the pyrrole β-substituted heme to develop a superior heme catalyst. The high reactivity of the *meso*-substituted heme would make the oxidation of a more inactive substrate possible. Since the *meso*-position of the heme tends to be more susceptible than the pyrrole β-position for the substitution reaction, as can be seen in the heme oxygenase reaction and the nitration reaction of heme,[53,54] the *meso*-substituted heme would be more sustainable than the pyrrole-β-substituted heme for the heme degradation reaction in the catalytic reactions. Moreover, the *meso*-substituted heme is easier to synthesize than the pyrrole β-substituted heme, facilitating the modification and/or functionalization of heme.

Most heme enzymes in nature have protoporphyrin IX or its derivatives, which can be classified into the pyrrole-β-substituted porphyrin, in their active sites. Therefore, the intrinsic reactivity of Compound I in native heme enzymes would be close to that of **TMTMP-I**, rather than **TMP-I**. The pyrrole-β-substituted structures of the hemes are favorable for peroxidases because the Compounds I in peroxidases catalyze the single electron transfer reaction from the substrate to Compound I.[55] On the other hand, the pyrrole-β-substituted structures of the hemes in cytochromes P450 and catalases are unfavorable because compounds I of these enzymes catalyze the O-atom and H-atom transfer reactions.[55−57] This disadvantage would be compensated by other inherent factors in their heme enzymes. The first one is the axial ligand; cytochrome P450 and catalase have a thiolate axial ligand from cysteine and a phenolate axial ligand from tyrosine, respectively. The σ-donor ability of these axial ligands is stronger than the axial ligand of peroxidase (histidine), because the pK_a values of thiol and phenol are larger than that of imidazole. Green et al. proposed that the strong binding of the thiolate axial ligand in cytochrome P450 increases the pK_a of the oxo ligand of Compound II, enhancing the H-atom abstraction ability. We revealed in a previous study using synthetic Compound I model complexes that, as the binding of the axial ligand is stronger, Compound I changes to being more reactive for the O-atom and H-atom transfer reactions. Moreover, the interactions of the heme with amino acid residues in the heme pocket would also assist in keeping the reactivity very high. The flexibility of the heme is decreased by the interactions of the heme in the heme pockets, such as hydrogen bonds and steric interaction. The binding site of a substrate, which fixes the substrate not to fluctuate and to be placed near the oxo ligand of Compound I, also assists in stabilizing the transition state.

EXPERIMENTAL SECTION

Instrumentation. UV−vis absorption spectra were recorded on an Agilent 8454 spectrometer (Agilent Technologies) equipped with a USP-203 low-temperature chamber (UNISOKU). ^{1}H NMR spectra were measured on a Lambda-400 spectrometer (JEOL). The chemical shifts were referenced to the residual peaks of the deuterated solvents chloroform (7.24 ppm) and toluene−CH_3 (2.09 ppm). The

https://dx.doi.org/10.1021/acs.inorgchem.0c03548
Inorg. Chem. 2021, 60, 3207−3217

concentrations of the NMR samples were 1−3 mM. The reaction product analyses were performed using a GC-MS QP-2010 SE gas chromatograph mass spectrometer (Shimadzu) or high-performance liquid chromatography (HPLC) LC-10AT system with a multidiode array detector (Shimadzu), attached to an octadodecylsilyl (ODS) column, 4.6 mm × 250 mm (SHISEIDO). Ozone gas was generated by the UV irradiation of oxygen gas (99.999%) with a PR-1300 ozone generator (Clear Water) and used without further purification. The kinetic analyses for fast reactions were performed using a stopped-flow rapid mixing system USP-R100 (UNISOKU) with a low-temperature double mixer USP-SFM-CRD10 (UNISOKU).

Materials. Anhydrous organic solvents were obtained commercially and stored in a glovebox. Dichloromethane was purified by passing through an alumina column just before use in the glovebox. Other chemicals were purchased commercially and used without further purification. TMP and TMTMP were synthesized by reported methods.[58] Syntheses of iron(III) complexes of TMP and TMTMP were described in a previous report.[59] Substrates for the reactions are purified by passing through active alumina just before use. Deuterium labeled *N*,*N*-dimethyl-*p*-nitroaniline was prepared from the reaction of *p*-nitroaniline with deuterium labeled methyl iodide (99.5% D).[60]

Kinetic Analysis: General Procedure. The ferric porphyrin complex (100 μM) in dichloromethane was prepared in a 1 cm quartz cuvette in a low-temperature chamber set on a UV−vis absorption spectrometer. After stabilization of the temperature of the solution at −50 °C, O_3 gas was slowly bubbled into the solution with a gastight syringe. The oxidation process was monitored using the absorption spectrometer. After confirming the generation of the oxoiron(IV) porphyrin π-cation radical complex, the excess O_3 gas in the cell was removed by bubbling argon gas with a gastight syringe. An excess of substrate (more than 10 equiv) was then added to the solution with stirring, and the progress of the reaction was followed at a constant time interval using absorption spectroscopy. The reaction rate constants were determined by simulation of the time course of the absorbance of the peaks with the commercial program Igor Pro 7 (WaveMetrics). The absorption spectral change followed the first-order kinetics in the presence of a large excess of the substrate, and the second-order reaction rate constants (k_2) were determined from the linear dependence of the pseudo-first-order rate constant on the concentration of the substrate.

Product Analysis: General/Typical Procedure. The ferric porphyrin complex (1.0 mM) in dichloromethane (0.22 mL) was prepared in a Schlenk flask and cooled to −50 °C in a temperature-controlled cooling bath. Ozone gas was slowly bubbled into the solution until the formation of the Compound I model complexes. The excess ozone gas was removed by the freeze−thaw method. Excess substrate (10 equiv) dissolved in dichloromethane was added to the solution at −50 °C. After completion of the reactions (~30 min), the reaction products and their yields were analyzed with GC-MS. The assignments of the products were performed on the basis of the retention times and the mass numbers of the authentic samples. The product yields of *N*-methylaniline and *N*-methyl-*p*-nitroaniline from the demethylation reactions of *N*,*N*-dimethylaniline and *N*,*N*-dimethyl-*p*-nitroaniline were analyzed by HPLC with an ODS column (4.6 mm × 250 mm) using an acetonitrile−water (8:2) mixture as an eluent.

Stopped-Flow Rapid Mixing Experiments: General Procedure. The iron(III) complex of TMP or TMTMP (~50 μM) was prepared in dichloromethane. The solution of iron(III) porphyrin and *m*-chloroperoxybenzoic acid (5 equiv) was placed in sample holders of a stopped flow and cooled at −20 °C. After cooling for 1 min, the solutions were rapidly mixed. After aging the mixture until the formation of Compound I (10−60 s), a solution of substrate (*N*,*N*-dimethylanilines or *tert*-butyl methyl sulfide) was further rapidly mixed to initiate the reaction. The reactions were monitored by the absorption spectral change at constant time intervals. The reaction rate constants were determined by simulation of the time course of the absorbance of the peaks. The second-order reaction rate constant (k_2) were determined from the linear dependence of the pseudo-first-order rate constant on the concentration of the substrate.

DFT Calculations. The DFT calculations were performed using the Gaussion09 program package. All basis sets were taken from the Gaussian09 program. We used two combinations of the DFT functional and basis set. LC-BLYP was used with cc-pVTZ for the O═Fe—Cl and the C and N atoms in porphyrin ring and sto-6g for the porphyrin substituents (mesityl group and methyl group). All compounds were fully optimized in the ground state of each spin multiplicity.

■ ASSOCIATED CONTENT

Supporting Information

The Supporting Information is available free of charge at https://pubs.acs.org/doi/10.1021/acs.inorgchem.0c03548.

Kinetic analyses and data from DFT calculations and additional data and figures including absorption spectral changes, optimized structures, spin distribution, bond lengths and angles, and molecular orbital energies (PDF)

■ AUTHOR INFORMATION

Corresponding Author

Hiroshi Fujii − *Department of Chemistry, Graduate School of Humanities and Sciences, Nara Women's University, Kitauoyanishi, Nara 630-8506, Japan;* orcid.org/0000-0003-4611-2983; Email: fujii@cc.nara-wu.ac.jp

Authors

Nami Fukui − *Department of Chemistry, Graduate School of Humanities and Sciences, Nara Women's University, Kitauoyanishi, Nara 630-8506, Japan*

Kanako Ueno − *Department of Chemistry, Graduate School of Humanities and Sciences, Nara Women's University, Kitauoyanishi, Nara 630-8506, Japan*

Masahiko Hada − *Department of Chemistry, Graduate School of Science, Tokyo Metropolitan University, Hachioji 192-0397, Japan;* orcid.org/0000-0003-2752-2442

Complete contact information is available at: https://pubs.acs.org/10.1021/acs.inorgchem.0c03548

Notes

The authors declare no competing financial interest.

■ ACKNOWLEDGMENTS

This study was supported by grants from JSPS (Grant 17H03032 and 19H04581) and CREST.

■ REFERENCES

(1) Huang, X.; Groves, J. T. Oxygen Activation and Radical Transformations in Heme Proteins and Metalloporphyrins. *Chem. Rev.* **2018**, *118*, 2491−2553.

(2) Baglia, R. A.; Zaragoza, J. P. T.; Goldberg, D. P. Biomimetic Reactivity of Oxygen-Derived Manganese and Iron Porphyrinoid Complexes. *Chem. Rev.* **2017**, *117* (21), 13320−13352.

(3) Nam, W. High-Valent Iron(IV)−Oxo Complexes of Heme and Non-Heme Ligands in Oxygenation Reactions. *Acc. Chem. Res.* **2007**, *40*, 522−531.

(4) Rittle, J.; Green, M. T. Cytochrome P450 compound I: capture, characterization, and C-H bond activation kinetics. *Science* **2010**, *330*, 933−937.

(5) Fujii, H. Electronic structure and reactivity of high-valent oxo iron porphyrins. *Coord. Chem. Rev.* **2002**, *226*, 51−60.

(6) Fujii, H., Model Complexes of Heme Peroxidases. In *Heme Peroxidases*; Raven, E.; Dunford, B., Eds.; The Royal Society of Chemistry: London, 2016; pp 183−217.

(7) Rohde, J. U.; In, J. H.; Lim, M. H.; Brennessel, W. W.; Bukowski, M. R.; Stubna, A.; Munck, E.; Nam, W.; Que, L., Jr. Crystallographic and spectroscopic characterization of a nonheme Fe(IV)-O complex. *Science* **2003**, *299* (5609), 1037−9.
(8) Seo, M. S.; Kim, N. H.; Cho, K.-B.; So, J. E.; Park, S. K.; Clémancey, M.; Garcia-Serres, R.; Latour, J.-M.; Shaik, S.; Nam, W. A mononuclear nonheme iron(iv)-oxo complex which is more reactive than cytochrome P450 model compound I. *Chem. Sci.* **2011**, *2* (6), 1039.
(9) Sono, M.; Roach, M. P.; Coulter, E. D.; Dawson, J. H. Heme-Containing Oxygenases. *Chem. Rev.* **1996**, *96* (7), 2841−2888.
(10) Rittle, J.; Green, M. T. Cytochrome P450 compound I: capture, characterization, and C-H bond activation kinetics. *Science* **2010**, *330* (6006), 933−7.
(11) Takahashi, A.; Kurahashi, T.; Fujii, H. Effect of Imidazole and Phenolate Axial Ligands on the Electronic Structure and Reactivity of Oxoiron(IV) Porphyrin π-Cation Radical Complexes: Drastic Increase in Oxo-Transfer and Hydrogen Abstraction Reactivities. *Inorg. Chem.* **2009**, *48*, 2614−2625.
(12) Takahashi, A.; Yamaki, D.; Ikemura, K.; Kurahashi, T.; Ogura, T.; Hada, M.; Fujii, H. Effect of the axial ligand on the reactivity of the oxoiron(IV) porphyrin π-cation radical complex: higher stabilization of the product state relative to the reactant state. *Inorg. Chem.* **2012**, *51* (13), 7296−305.
(13) Prokop, K. A.; de Visser, S. P.; Goldberg, D. P. Unprecedented rate enhancements of hydrogen-atom transfer to a manganese(V)-oxo corrolazine complex. *Angew. Chem., Int. Ed.* **2010**, *49* (30), 5091−5.
(14) Traylor, P. S.; Dolphin, D.; Traylor, T. G. Sterically protected hemins with electronegative substituents: efficient catalysts for hydroxylation and epoxidation. *J. Chem. Soc., Chem. Commun.* **1984**, 279−280.
(15) Gold, A.; Jayaraj, K.; Doppelt, P.; Weiss, R.; Chottard, G.; Bill, E.; Ding, X.; Trautwein, A. X. Oxoferryl complexes of the halogenated (porphinato)iron catalyst [tetrakis(2,6-dichlorophenyl)porphinato]-iron. *J. Am. Chem. Soc.* **1988**, *110* (17), 5756−5761.
(16) Fujii, H. Effects of the electron-withdrawing power of substituents on the electronic structure and reactivity in oxoiron(IV) porphyrin π-cation radical complexes. *J. Am. Chem. Soc.* **1993**, *115* (11), 4641−4648.
(17) Goh, Y. M.; Nam, W. Significant Electronic Effect of Porphyrin Ligand on the Reactivities of High-Valent Iron(IV) Oxo Porphyrin Cation Radical Complexes. *Inorg. Chem.* **1999**, *38* (5), 914−920.
(18) Collins, T. J.; Ryabov, A. D. Targeting of High-Valent Iron-TAML Activators at Hydrocarbons and Beyond. *Chem. Rev.* **2017**, *117* (13), 9140−9162.
(19) Ishimizu, Y.; Ma, Z.; Hada, M.; Fujii, H. Experimental and theoretical studies of the porphyrin ligand effect on the electronic structure and reactivity of oxoiron(iv) porphyrin π-cation-radical complexes. *JBIC, J. Biol. Inorg. Chem.* **2019**, *24* (4), 483−494.
(20) Afanasiev, P.; Sorokin, A. B. μ-Nitrido Diiron Macrocyclic Platform: Particular Structure for Particular Catalysis. *Acc. Chem. Res.* **2016**, *49* (4), 583−93.
(21) Kumar, D.; Tahsini, L.; de Visser, S. P.; Kang, H. Y.; Kim, S. J.; Nam, W. Effect of porphyrin ligands on the regioselective dehydrogenation versus epoxidation of olefins by oxoiron(IV) mimics of cytochrome P450. *J. Phys. Chem. A* **2009**, *113* (43), 11713−22.
(22) Sugimoto, H.; Tung, H. C.; Sawyer, D. T. The formation, characterization, and reactivity of the oxene adduct of [tetrakis(2,6-dichlorophenyl)porphinato]iron(III) perchlorate in acetonitrile. Model for the reactive intermediate of cytochrome P-450. *J. Am. Chem. Soc.* **1988**, *110* (8), 2465−2470.
(23) Fujii, H. Characterization of High Valent Iron Porphyrin in Catalytic Reaction by Iron(III) Tetrapentafluorophenylporphyrin. *Chem. Lett.* **1994**, *23*, 1491−1494.
(24) Song, W. J.; Ryu, Y. O.; Song, R.; Nam, W. Oxoiron(IV) porphyrin π-cation radical complexes with a chameleon behavior in cytochrome P450 model reactions. *JBIC, J. Biol. Inorg. Chem.* **2005**, *10*, 294−304.
(25) Che, C. M.; Zhang, J. L.; Zhang, R.; Huang, J. S.; Lai, T. S.; Tsui, W. M.; Zhou, X. G.; Zhou, Z. Y.; Zhu, N.; Chang, C. K. Hydrocarbon oxidation by beta-halogenated dioxoruthenium(VI) porphyrin complexes: effect of reduction potential (RuVI/V) and C-H bond-dissociation energy on rate constants. *Chem. - Eur. J.* **2005**, *11* (23), 7040−53.
(26) Porhiel, E.; Bondon, A.; Leroy, J. (β-Octafluoro-meso-tetraarylporphyrin)manganese Complexes: Synthesis, Characterization and Catalytic Behaviour in Monooxygenation Reactions. *Eur. J. Inorg. Chem.* **2000**, *2000* (5), 1097−1105.
(27) Garrison, J. M.; Ostovic, D.; Bruice, T. C. Is a linear relationship between the free energies of activation and one-electron oxidation potential evidence for one-electron transfer being rate determining? Intermediates in the epoxidation of alkenes by cytochrome P-450 models. 4. Epoxidation of a series of alkenes by oxo(meso-tetrakis(2,6-dibromophenyl)porphinato)chromium(V). *J. Am. Chem. Soc.* **1989**, *111* (13), 4960−4966.
(28) Asaka, M.; Fujii, H. Participation of Electron Transfer Process in Rate-Limiting Step of Aromatic Hydroxylation Reactions by Compound I Models of Heme Enzymes. *J. Am. Chem. Soc.* **2016**, *138* (26), 8048−51.
(29) Takahashi, A.; Kurahashi, T.; Fujii, H. Redox potentials of oxoiron(IV) porphyrin π-cation radical complexes: participation of electron transfer process in oxygenation reactions. *Inorg. Chem.* **2011**, *50*, 6922−8.
(30) Bhyrappa, P.; Young, J. K.; Moore, J. S.; Suslick, K. S. Dendrimer-Metalloporphyrins: Synthesis and Catalysis. *J. Am. Chem. Soc.* **1996**, *118* (24), 5708−5711.
(31) Groves, J. T.; Viski, P. Asymmetric hydroxylation by a chiral iron porphyrin. *J. Am. Chem. Soc.* **1989**, *111* (22), 8537−8538.
(32) Sainna, M. A.; Kumar, S.; Kumar, D.; Fornarini, S.; Crestoni, M. E.; de Visser, S. P. A comprehensive test set of epoxidation rate constants for iron(iv)-oxo porphyrin cation radical complexes. *Chem. Sci.* **2015**, *6* (2), 1516−1529.
(33) Groves, J. T.; Haushalter, R. C.; Nakamura, M.; Nemo, T. E.; Evans, B. J. High-valent iron-porphyrin complexes related to peroxidase and cytochrome P-450. *J. Am. Chem. Soc.* **1981**, *103* (10), 2884−2886.
(34) Fujii, H.; Ichikawa, K. Preparation and characterization of an A1u Oxoiron(IV) porphyrin π-cation-radical complex. *Inorg. Chem.* **1992**, *31* (6), 1110−1112.
(35) Fukui, N.; Li, X. X.; Nam, W.; Fukuzumi, S.; Fujii, H. Small Reorganization Energy for Ligand-Centered Electron-Transfer Reduction of Compound I to Compound II in a Heme Model Study. *Inorg. Chem.* **2019**, *58* (13), 8263−8266.
(36) Cong, Z.; Kinemuchi, H.; Kurahashi, T.; Fujii, H. Factors Affecting Hydrogen-Tunneling Contribution in Hydroxylation Reactions Promoted by Oxoiron(IV) Porphyrin π-Cation Radical Complexes. *Inorg. Chem.* **2014**, *53* (19), 10632−41.
(37) Goto, Y.; Matsui, T.; Ozaki, S.; Watanabe, W.; Fukuzumi, S. Mechanisms of Sulfoxidation Catalyzed by High-Valent Intermediates of Heme Enzymes: Electron-Transfer vs Oxygen-Transfer Mechanism. *J. Am. Chem. Soc.* **1999**, *121*, 9497−9502.
(38) Goto, Y.; Watanabe, Y.; Fukuzumi, S.; Jones, J. P.; Dinnocenzo, J. P. Mechanisms of N-Demethylations Catalyzed by High-Valent Species of Heme Enzymes: Novel Use of Isotope Effects and Direct Observation of Intermediates. *J. Am. Chem. Soc.* **1998**, *120*, 10762−10763.
(39) Fujii, H.; Yoshimura, T.; Kamada, H. ESR Studies of A1u and A2u Oxoiron(IV) Porphyrin π-Cation Radical Complexes. Spin Coupling between Ferryl Iron and A1u/A2u Orbitals. *Inorg. Chem.* **1996**, *35* (8), 2373−2377.
(40) Groves, J. T.; McClusky, G. A. Aliphatic Hydroxylation via Oxygen Rebound. Oxygen Transfer Catalyzed by Iron. *J. Am. Chem. Soc.* **1976**, *98*, 859−861.
(41) Zaragoza, J. P. T.; Yosca, T. H.; Siegler, M. A.; Moenne-Loccoz, P.; Green, M. T.; Goldberg, D. P. Direct Observation of Oxygen Rebound with an Iron-Hydroxide Complex. *J. Am. Chem. Soc.* **2017**, *139* (39), 13640−13643.

https://dx.doi.org/10.1021/acs.inorgchem.0c03548
Inorg. Chem. 2021, 60, 3207−3217

(42) Hjelmeland, L. M.; Aronow, L.; Trudell, J. R. Intramolecular determination of primary kinetic isotope effects in hydroxylations catalyzed by cytochrome P-450. *Biochem. Biophys. Res. Commun.* **1977**, *76* (2), 541−549.
(43) Jones, J. P.; Trager, W. F. The separation of the intramolecular isotope effect for the cytochrome P-450 catalyzed hydroxylation of n-octane into its primary and secondary components. *J. Am. Chem. Soc.* **1987**, *109* (7), 2171−2173.
(44) Kadkhodayan, S.; Coulter, E. D.; Maryniak, D. M.; Bryson, T. A.; Dawson, J. H. Uncoupling oxygen transfer and electron transfer in the oxygenation of camphor analogues by cytochrome P450-CAM. Direct observation of an intermolecular isotope effect for substrate C-H activation. *J. Biol. Chem.* **1995**, *270* (47), 28042−8.
(45) Groves, J. T.; Adhyam, D. V. Hydroxylation by cytochrome P-450 and metalloporphyrin models. Evidence for allylic rearrangement. *J. Am. Chem. Soc.* **1984**, *106* (7), 2177−2181.
(46) Groves, J. T.; Nemo, T. E. Aliphatic hydroxylation catalyzed by iron porphyrin complexes. *J. Am. Chem. Soc.* **1983**, *105* (20), 6243−6248.
(47) Jeong, Y. J.; Kang, Y.; Han, A. R.; Lee, Y. M.; Kotani, H.; Fukuzumi, S.; Nam, W. Hydrogen atom abstraction and hydride transfer reactions by iron(IV)-oxo porphyrins. *Angew. Chem., Int. Ed.* **2008**, *47*, 7321−4.
(48) Sorokin, A.; Robert, A.; Meunier, B. Intramolecular kinetic isotope effects in alkane hydroxylations catalyzed by manganese and iron porphyrin complexes. *J. Am. Chem. Soc.* **1993**, *115* (16), 7293−7299.
(49) Pan, Z.; Horner, J. H.; Newcomb, M. Tunneling in C-H oxidation reactions by an oxoiron(IV) porphyrin radical cation: direct measurements of very large H/D kinetic isotope effects. *J. Am. Chem. Soc.* **2008**, *130* (25), 7776−7.
(50) Groves, J. T.; Nemo, T. E. Epoxidation reactions catalyzed by iron porphyrins. Oxygen transfer from iodosylbenzene. *J. Am. Chem. Soc.* **1983**, *105* (18), 5786−5791.
(51) Traylor, T. G.; Nakano, T.; Dunlap, B. E.; Traylor, P. S.; Dolphin, D. Mechanisms of hemin-catalyzed alkene epoxidation. The effect of catalyst on the regiochemistry of epoxidation. *J. Am. Chem. Soc.* **1986**, *108* (10), 2782−2784.
(52) Collman, J. P.; Brauman, J. I.; Meunier, B.; Raybuck, S. A.; Kodadek, T. Epoxidation of olefins by cytochrome P-450 model compounds: mechanism of oxygen atom transfer. *Proc. Natl. Acad. Sci. U. S. A.* **1984**, *81* (10), 3245−8.
(53) Fujii, H.; Zhang, X.; Tomita, T.; Ikeda-Saito, M.; Yoshida, T. A Role for Highly Conserved Carboxylate, Aspartate-140, in Oxygen Activation and Heme Degradation by Heme Oxygenase-1. *J. Am. Chem. Soc.* **2001**, *123*, 6475−6484.
(54) Bonnett, R.; Stephenson, G. F. The meso Reactivity of Porphyrins and Related Compounds. I. Nitration. *J. Org. Chem.* **1965**, *30* (8), 2791−2798.
(55) Dunford, H. B. Historical: Poineering work on Horseradish and Yeast Cyochrome c Peroxidases. In *Peroxidases and Catalases*; Dubford, H. B., Ed.; John Wiley & Sons: New Jersey, 2010; pp 1−8.
(56) Munro, A. W.; McLean, K. J.; Grant, J. L.; Makris, T. M. Structure and function of the cytochrome P450 peroxygenase enzymes. *Biochem. Soc. Trans.* **2018**, *46* (1), 183−196.
(57) Ortiz de Montellano, P. R. Mechanism and role of covalent heme binding in the CYP4 family of P450 enzymes and the mammalian peroxidases. *Drug Metab. Rev.* **2008**, *40* (3), 405−26.
(58) Ono, N.; Kawamura, H.; Bougauchi, M.; Maruyama, K. Porphyrin synthesis from nitrocompounds. *Tetrahedron* **1990**, *46* (21), 7483−7496.
(59) Yokota, S.; Fujii, H. Critical Factors in Determining the Heterolytic versus Homolytic Bond Cleavage of Terminal Oxidants by Iron(III) Porphyrin Complexes. *J. Am. Chem. Soc.* **2018**, *140* (15), 5127−5137.
(60) Monaco, A.; Zoete, V.; Alghisi, G. C.; Ruegg, C.; Michelin, O.; Prior, J.; Scapozza, L.; Seimbille, Y. Synthesis and in vitro evaluation of a novel radioligand for alphavbeta3 integrin receptor imaging: [18F]FPPA-c(RGDfK). *Bioorg. Med. Chem. Lett.* **2013**, *23* (22), 6068−6072.

https://dx.doi.org/10.1021/acs.inorgchem.0c03548
Inorg. Chem. 2021, 60, 3207−3217